CCFE
CULHAM CENTRE FOR FUSION ENERGY

UK Atomic Energy Authority

UKAEA-CCFE-PR(21)69

P. Ollus, R. Akers, H. El-Haroun, D. Keeling, T. Kurki-Suonio, R. Sharma, A. Snicker, J. Varje, MAST-U Team, MST1 Team

Simulating the impact of charge exchange on beam ions in MAST-U

Simulating the impact of charge exchange on beam ions in MAST-U

P. Ollus, R. Akers, H. El-Haroun, D. Keeling, T. Kurki-Suonio, R. Sharma, A. Snicker, J. Varje, MAST-U Team, MST1 Team

This is a preprint of a paper submitted for publication in Plasma Physics and Controlled Fusion

Simulating the impact of charge exchange on beam ions in MAST-U

P. Ollus[a,*], R. Akers[b], B. Colling[b], H. El-Haroun[b], D. Keeling[b], T. Kurki-Suonio[a], R. Sharma[b], A. Snicker[a], J. Varje[a,**], the MAST-U team[1], the EUROfusion MST1 team[2]

[a] *Department of Applied Physics, Aalto University, P.O. Box 11100, 00076 AALTO, Finland*
[b] *Culham Centre for Fusion Energy, Culham Science Centre, Abingdon, OX14 3DB, United Kingdom of Great Britain and Northern Ireland*

Abstract

A model for simulating charge exchange (CX) of fast ions with background atoms in magnetically confined fusion plasmas has been implemented in the ASCOT orbit-following code. The model was verified by comparing simulated reaction mean free paths to analytical values across a range of fusion-relevant parameters.

ASCOT was used to simulate beam ions slowing down in the presence of CX reactions in a MAST-U target scenario. ASCOT predicts the CX-induced loss of beam power to be 22%, which agrees to within 15% with the TRANSP prediction. Because of CX, plasma heating and current drive by beam ions are strongly reduced towards the edge. However, an overall lower but noticeable increase of up to 20% in current drive is predicted closer to the core. The simulated deposition of fast CX atoms on the wall is concentrated around the outer midplane, with estimated peak power loads of 70–80 kWm^{-2} on the central poloidal field coils (P5) and the vacuum vessel wall between them. This analysis demonstrates that ASCOT can be used to simulate fast ions in fusion plasmas where CX reactions play a significant role, e.g., in spherical tokamaks and stellarators.

1. Introduction

Charge-exchange (CX) reactions with background neutrals have been shown to have caused significant beam-ion losses in MAST [1], and the same issue is likely to arise in MAST-U. CX losses of beam ions result in the loss of heating power and current drive. In addition, escaping fast particles damage sensitive plasma-facing components and cause impurity sputtering and wall erosion. To address the impact of CX on fast ions in MAST-U and other devices, a new model for CX reactions has been implemented in the fast-ion orbit-following code ASCOT [2]. The model extends the applicability of ASCOT to the simulation of fast ions in fusion plasmas where CX reactions play a significant role, e.g., in spherical tokamaks and stellarators.

The topic of fast-ion CX losses has been under active research in recent years with various fast-ion orbit-following codes. The NSS OFMC code [3] was used to show that CX losses of fast ions had a significant impact on the neutron rate in MAST [1]. The SPIRAL code [4] was used to simulate fast-ion losses induced by CX with neutrals in the scrape-off layer in tokamaks [5]. The EBdyna code was used to model CX losses of beam ions for the design activities of the COMPASS upgrade tokamak [6]. The transport code TRANSP [7, 8], with its guiding-center fast-ion module NUBEAM [9], has also been used to estimate fast-ion CX losses [10] in MAST.

The ASCOT CX model extends the existing capabilities for modelling fast-ion CX. Previous work on modelling the neutron rate in MAST suggests that it is necessary to follow the full gyro-orbits of fast ions to accurately reproduce experiments in the spherical tokamak geometry [3, 11]. The full gyro-orbit following capabilities of ASCOT combined with its near-optimal scaling on supercomputers allows high-fidelity simulation of fast-ion populations in high-∇B geometries, such as the spherical MAST-U tokamak. None of the other codes mentioned above have demonstrated the ability to simulate CX-induced localized wall loads on a physical 3D wall representation or the ability to simulate fast-ion CX in stellarators. Since ASCOT markers, charged or neutral, are followed to an arbitrarily detailed 3D wall representation, global and localized wall power loads are estimated. The applicability of ASCOT for modelling fast ions in stellarators has been well established [12], and its new ability to simulate fast-ion CX reactions can be included in stellarator modelling. Furthermore, there is no literature pertaining to the simulation of fast-ion transport due to the combined effects of CX reactions and magnetohydrodynamic (MHD) instabilities. Given the existing versatility of the ASCOT code, the simulation of fast-ion CX can be combined with the simulation of other processes, such as MHD instabilities.

In this article, we introduce the new CX model of the ASCOT code, its testing and demonstrative results regarding the impact of CX on beam ions in MAST-U. Section 2

*Corresponding author
**Current affiliation: *Tokamak Energy Ltd., 173 Brook Dr, Milton Park, Abingdon, UK*
Email address: patrik.ollus@aalto.fi (P. Ollus)
[1] See the author list of J. Harrison et al. 2019 Nucl. Fusion, 59 112011
[2] See the author list of B. Labit et al. 2019 Nucl. Fusion 59 086020

describes the CX model. The verification of the model by estimation of reaction mean free paths is reported in section 3. Section 4 reports on the simulation of beam-ion CX in MAST-U, including scenario description, analysis of results and comparison to TRANSP. A summary is given, conclusions drawn and future work discussed in section 5.

2. Simulating charge exchange for fast ions

Fast ions in magnetic confinement fusion devices are subject to neutralization by CX with background atoms and the subsequent reionization by the bulk plasma [5]. The established Monte Carlo orbit-following code ASCOT [2], which is used to simulate minority particles in magnetic confinement fusion devices, has been expanded with a module for simulating such atomic processes for fast ions. The neutralization of hydrogenic fast ions through CX with hydrogenic background atoms and the possible reionization of the fast CX atoms by the bulk plasma have been implemented, constituting a model for the simulation of fast-ion CX.

In the ASCOT CX model, neutralization into the ground state of hydrogenic fast ions through CX with hydrogenic background atoms in the ground state is simulated using fundamental cross-section data. For the simulations reported here, cross-sections that depend on collision energy were imported from the Atomic Data and Analysis Structure (ADAS) [13, 14, 15], specifically the ADAS data format ADF24. During ASCOT initialization, the cross-sections are transformed through Maxwellian averaging [15, 16] into rate coefficients, which depend on fast-ion energy and atomic temperature. The background atoms are assumed Maxwellian at the ion temperature, a common approximation due to frequent CX between bulk particles [17, 18]. The atomic background is currently limited to one species with a 1D density profile[3], which is given as input. Upon their neutralization, markers are followed using a ballistic model until they are reionized or hit the wall.

Reionization is simulated using effective beam stopping (BMS) coefficients. This class of rate coefficients, originally designed for beam attenuation calculations, depends on fast-particle energy and plasma density and temperature. BMS coefficients can be imported from the ADAS database or calculated using analytical fits built into ASCOT [20]. For the simulations reported here, BMS coefficients were imported from ADF21 [21], specifically coefficients produced in the year 2010 [22] for a hydrogenic plasma and in 1997 for fully ionized carbon impurities. The plasma densities and temperature, needed to evaluate the BMS coefficient, are included among the standard ASCOT inputs.

[3] ASCOT4 [2], used in this work, is limited to a 1D atomic density profile. ASCOT5 [19] supports a 3D atomic density distribution, which is currently in testing.

Like other ASCOT inputs, all atomic data grids are interpolated using cubic splines [23]. If the fast-particle energy or plasma or atomic density or temperature are outside the domain of the atomic data, linear extrapolation is used to approximate a value. The relevance of out-of-domain parameter spaces must be assessed case-specifically to estimate possible resulting uncertainties. The inter- and extrapolation methods that ASCOT applies to the atomic data imported from ADAS are not to be confused with the inter- and extrapolation of experimental and theoretical data by ADAS in the generation of atomic data, such as the cross-sections from ADF24.

During the ASCOT simulation of a marker time step, once the reaction rate coefficient ($\mathrm{m^3 s^{-1}}$) has been evaluated for the current particle state and plasma conditions, it is multiplied by the reaction counterpart density to yield the reaction rate ($\mathrm{s^{-1}}$). The reaction rate is used to calculate the probability for a reaction to occur during the current time step. The probability is tested against a uniformly distributed random number between 0 and 1 [24]. If a reaction occurs, the particle charge state is changed, taking effect at the start of the next time step. More details about the ASCOT atomic processes module are given in [25].

3. Verification by mean free path estimation

To verify the correct implementation of the ASCOT fast-ion CX model, specifically the Maxwellian averaging of CX cross-sections, the interpolation of atomic data and the probabilistic reaction algorithm, ASCOT was used to estimate reaction mean free paths. The estimates were compared to the independently calculated analytical mean free paths,

$$d_{MFP} = \frac{u}{\mathcal{R}} = \frac{u}{\langle \sigma v \rangle n},$$

where u is the fast-particle speed, $\mathcal{R}$ the reaction rate, $\langle \sigma v \rangle$ the reaction rate coefficient, and n the reaction counterpart density.

The mean-free-path test was performed for the neutralization of fast deuterons through CX with thermal deuterium atoms, and for the ionization of fast deuterium atoms in two different plasmas, one of deuterons and one of fully ionized carbon. To simplify the calculation, Coulomb collisions were turned off to conserve particle energy, and the plasma and atomic density and temperature profiles were equal for all species and constant throughout the simulation domain. For each mean-free-path estimate, 100 000 markers were simulated until undergoing a reaction. The analytical mean free paths, including the intermediate step of Maxwellian averaging of CX cross-sections into rate coefficients, were calculated independently of ASCOT. The CX cross-sections were interpolated using cubic interpolation, and the CX rate coefficients and the BMS coefficients were interpolated using splines. The tests were repeated at different orders of magnitude of each of the parameters:

fast-particle energy E, and atomic density n_0 and temperature T_0 or plasma density and temperature. The plasma density is given in terms of equivalent electron density n_e, as is convention in ADAS. The electron temperature T_e equals the ion temperature. The energy and temperature values were chosen to reflect a range of values typically present in current-day fusion plasmas, for example those planned for MAST-U. For convenience, the density values were chosen from the upper end of the range of values featured in existing fusion devices. Mean free paths were calculated for all combinations of the different parameter values.

Comparisons of the ASCOT-estimated and analytically calculated mean free paths for the CX reaction and the two ionization reactions are shown in tables 1, 2 and 3, respectively. All estimates match the analytical values within margins of standard error, verifying the correct implementation of the model.

Table 1: Mean free paths for the neutralization of a fast deuteron through CX with a thermal deuterium atom. Estimates by ASCOT using 100 000 markers are compared to analytical values.

E (keV)	n_0 (m^{-3})	T_0 (keV)	Mean free path (m)	
			ASCOT	analytical
10	10^{16}	0.1	909 ± 2.9	908
10	10^{16}	1	925 ± 2.9	924
10	10^{17}	0.1	90.9 ± 0.29	90.8
10	10^{17}	1	92.5 ± 0.29	92.4
100	10^{16}	0.1	10060 ± 32	10040
100	10^{16}	1	9940 ± 31	9920
100	10^{17}	0.1	1006 ± 3.2	1004
100	10^{17}	1	994 ± 3.1	992

Table 2: Mean free paths for the ionization of a fast deuterium atom in a thermal deuteron plasma. Estimates by ASCOT using 100 000 markers are compared to analytical values.

E (keV)	n_e (m^{-3})	T_e (keV)	Mean free path (mm)	
			ASCOT	analytical
10	10^{20}	0.1	61.8 ± 0.20	61.7
10	10^{20}	1	70.6 ± 0.22	70.4
10	10^{21}	0.1	5.63 ± 0.018	5.62
10	10^{21}	1	6.43 ± 0.020	6.42
100	10^{20}	0.1	220.2 ± 0.70	219.9
100	10^{20}	1	251.2 ± 0.79	250.9
100	10^{21}	0.1	17.86 ± 0.056	17.83
100	10^{21}	1	20.37 ± 0.064	20.34

A known source of systematic error is the finite time step in ASCOT. Since reactions that occur during a time step are registered as occurring at the end of the time step, the free path might be overestimated, at most by the distance travelled during one time step. At the maximum particle energy in these tests, 100 keV, given the time steps used, 10^{-9} s in the CX tests and 10^{-13} s in the ionization tests, the distances travelled during one time step are $3 \cdot 10^{-3}$ m and $3 \cdot 10^{-4}$ mm, respectively. These upper limits for the systematic error from the finite time step are orders of magnitude smaller than the error margins shown in tables 1, 2 and 3, implying that the systematic error is insignificant in these tests.

Table 3: Mean free paths for the ionization of a fast deuterium atom in a thermal plasma of fully ionized carbon. Estimates by ASCOT using 100 000 markers are compared to analytical values.

E (keV)	n_e (m^{-3})	T_e (keV)	Mean free path (mm)	
			ASCOT	analytical
10	10^{20}	0.1	84.7 ± 0.27	84.5
10	10^{20}	1	90.6 ± 0.29	90.4
10	10^{21}	0.1	7.73 ± 0.024	7.71
10	10^{21}	1	8.27 ± 0.026	8.25
100	10^{20}	0.1	161.0 ± 0.51	160.5
100	10^{20}	1	172.2 ± 0.54	171.8
100	10^{21}	0.1	14.89 ± 0.047	14.85
100	10^{21}	1	15.93 ± 0.050	15.89

4. Simulating beam-ion charge exchange in MAST-U

ASCOT was used to simulate the full gyro-orbits of beam ions slowing down in the presence of CX reactions in a MAST-U target scenario. The goals were to predict the transport and loss of beam ions due to CX and estimate the impacts on plasma heating and current drive, as well as to estimate the resulting beam-particle power loads on the first wall. Predictions by ASCOT and TRANSP are compared where possible. The analysis demonstrates the capabilities of the ASCOT CX model.

4.1. Scenario inputs and approximations

The subject of study was the MAST-U high-density target scenario A.1: a double-null plasma with a 1.0 MA plasma current and two beams, one on-axis and one off-axis, with nominal injection energies of 75 keV and a combined injection power of 5.0 MW [26, 27]. The transport code TRANSP has been used extensively for predictive modelling of MAST-U. Scenario data for the construction of the ASCOT inputs was extracted from the MAST-U TRANSP database (simulation number 99999I38). The time point 5.5 s was chosen from towards the end of the TRANSP simulation when steady-state conditions had been reached.

The magnetic field, visualized in Fig. 1, has a strength of 2.2 T at the separatrix on the inner midplane, 0.70 T on the magnetic axis and 0.56 T at the separatrix on the outer midplane. The electron density, shown in Fig. 2, ranges from $7.3 \cdot 10^{19}$ m^{-3} in the core to $4.7 \cdot 10^{18}$ m^{-3} at the separatrix. The ion species are deuterons, protons and fully ionized carbon, which radially averaged correspond to 76%, 8.1% and 16% of the electron density, respectively. The electron and ion temperature, shown in Fig. 3, ranges from 1.1 keV in the core to 120 eV at the separatrix. The

thermal atomic density, which is assumed poloidally uniform and shown in Fig. 2, ranges from $1.5 \cdot 10^{13}$ m^{-3} to $5.0 \cdot 10^{17}$ m^{-3}. The highest value is reached at the separatrix and assumed throughout the scrape-off layer. Given the non-uniformity of plasma recycling from the wall, the assumption of a poloidally uniform atomic background is invalid and expected to cause considerable uncertainty in simulated fast-ion CX relative to experiment.

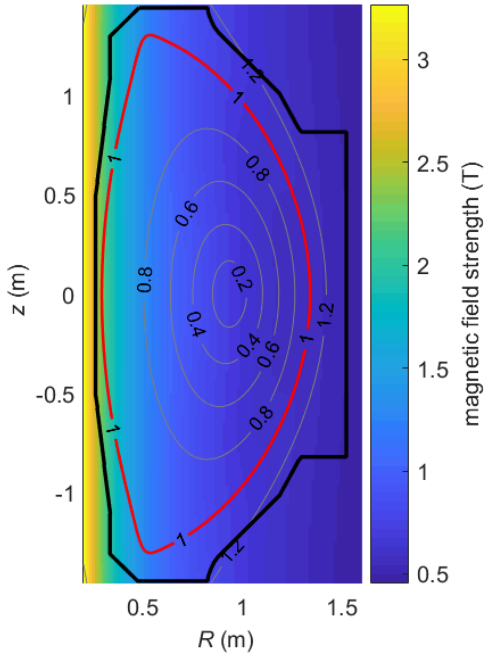

Figure 1: Total magnetic field strength, separatrix (red), other flux surfaces (gray) and reduced 2D wall (black) [28] in the Rz plane, where R is the major radius and z the vertical coordinate. The flux surfaces are labelled with the normalized poloidal flux $\rho_{\mathrm{pol}} = \sqrt{(\psi_{\mathrm{pol}} - \psi_{\mathrm{pol,ax}})/(\psi_{\mathrm{pol,sep}} - \psi_{\mathrm{pol,ax}})}$, where ψ_{pol} is the poloidal flux, and $\psi_{\mathrm{pol,ax}}$ and $\psi_{\mathrm{pol,sep}}$ are its values at the magnetic axis and inside the separatrix, respectively.

In this high-density scenario, the plasma captures practically all of the injected beam power. The TRANSP-predicted shine-through of the beam injection is only 4.8 kW, or 0.095% of the injected 5.0 MW. The ensemble of captured beam ions consists of 19 536 markers. The radial beam-ion birth profile is shown in Fig. 4.

The recreation of the TRANSP case for ASCOT required approximations. In TRANSP, the thermal atomic content is separated by species and source, each with its own density and temperature profiles. Radially averaged, the atomic background consists of 90% deuterium and 10% protium. Due to current limitations of ASCOT, the thermal atomic content was assumed to consist purely of deuterium and have a temperature equal to the ion temperature. The deuterium density used was the sum of the six density profiles of atoms in TRANSP, namely deuterium and protium recycled from the wall, born in the beam halo and born through recombination in the plasma.

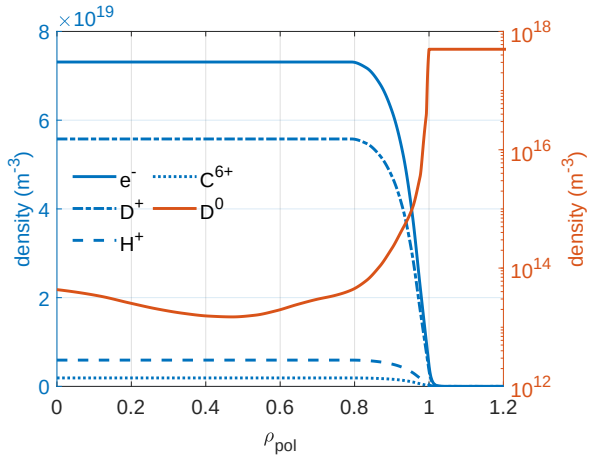

Figure 2: Radial density profiles of electrons (e^-), deuterons (D^+), protons (H^+), fully ionized carbon (C^{6+}) and atomic deuterium (D^0) as functions of the normalized poloidal flux coordinate ρ_{pol}.

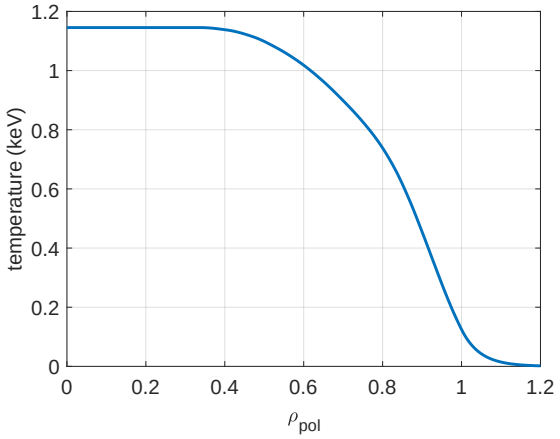

Figure 3: Radial temperature profile of electrons, ions and atoms.

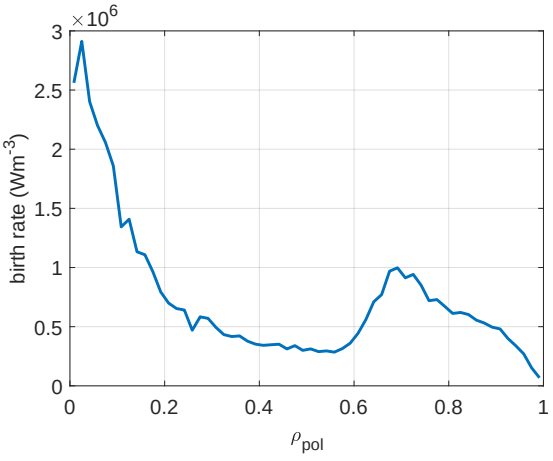

Figure 4: Radial beam-ion birth profile.

The rate coefficient for CX depends only modestly on the isotope mass and the temperature of the thermal reactant. By comparing the possible CX reaction rates inside the plasma with the simplified atomic background and that of TRANSP at energies of 1–80 keV, the simplified atomic background was found to retain the rates to within -1.1% and +2.4%. If the lower energy limit is increased to 10 keV, the uncertainty margins reduce to -0.34% and +0.22%. Hence, the above approximations are deemed good. While TRANSP includes the fast ions in the quasi-neutrality condition of its ion density, the ASCOT plasma is quasi-neutral with the thermal background ions alone.

The simple 2D wall contour shown in Fig. 1 was used in all ASCOT simulations except for one. In a simulation used to estimate the power loads on the MAST-U wall from beam particles lost due to CX, a detailed 3D wall representation consisting of 7 million triangles was used. To match the TRANSP marker ensemble to the resolution of the 3D wall, each marker was split into 30 identical markers, increasing the number of markers from 19 536 to 586 080. The magnetic background was extrapolated using splines to cover the entire interior of the 3D wall, a technical requirement of ASCOT. The unphysical nature of the extrapolation was not expected to be an issue, since markers reaching this far out of the plasma were expected to be neutral.

4.2. Charge-exchange losses

To further test the CX model of ASCOT, simulation results were compared to those of TRANSP. The TRANSP simulation used for this analysis was run using the upgraded version of the finite-Larmor-radius corrections [27, 29] and the newest atomic physics model (the module ADAS310_FORTRAN_DRIVER [29]).

ASCOT reproduces the general evolution of the beam-ion ensemble that TRANSP predicts. Figure 5 compares the predictions by ASCOT and TRANSP of the radial slowing-down density profiles of the beam ions. Between $\rho_{\mathrm{pol}} = 0.1$ and 0.9, the ASCOT prediction for the beam-ion density is within 5% of that of TRANSP. Towards the edge, the ASCOT prediction is lower, with an increasing relative difference that reaches 30% at the separatrix. It is worth noting that the absolute density is low close to the edge, implying a small contribution to the total beam-ion content and high statistical uncertainty relative to the rest of the plasma. Moreover, beam ions in the edge region are the ones most affected by CX. Since ASCOT and TRANSP agree on the general behaviour of the beam ion ensemble in the plasma, comparison specific to the effects of CX is possible.

In the absence of CX reactions, the beam ions in the analyzed case are well confined. An ASCOT simulation of the beam-ion ensemble with CX reactions turned off predicts that only 1.8 kW, or 0.036% of the captured beam power is lost through processes other than CX, such as neoclassical diffusion. Since these losses are negligible, all losses of beam ions in the presence of CX are considered to be caused by CX.

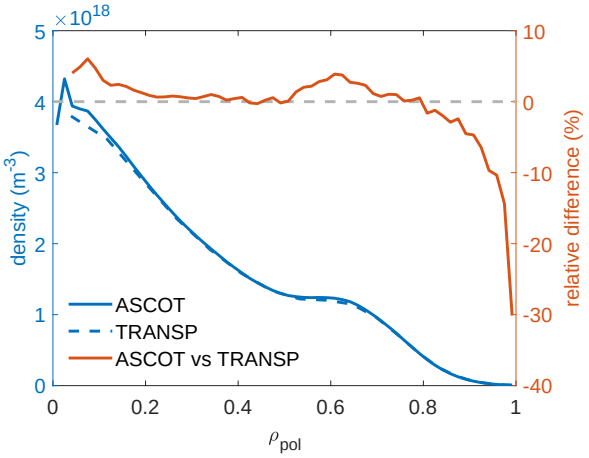

Figure 5: Radial slowing-down density profiles of beam ions simulated by ASCOT and TRANSP. The relative difference is shown on a separate scale.

A possible source of error in ASCOT is the finite time step, which might overestimate the reionization free path, which at relevant plasma densities and particle energies is of the order of tens or hundreds of millimeters, as shown in tables 2 and 3. The extremely short time step 10^{-13} s used for the ionization mean-free-path tests in section 3 is impractical for slowing-down simulations. In all slowing-down simulations except for the one with more markers and the 3D wall, the time step $2 \cdot 10^{-10}$ s was used. During that time, a deuterium atom with an energy of 75 keV travels 0.54 mm. Comparing to tables 2 and 3, this upper limit of the free-path error is 2–3 orders of magnitude shorter than the mean free path. Hence, this source of error is deemed negligible.

ASCOT predicts that 1.1 MW, or 22% of the captured beam power is lost from the plasma due to CX. This agrees to within 15% with TRANSP, which predicts that 19% of beam power is lost due to CX. According to ASCOT, 75% of the lost power originates from the off-axis beam. The energy spectrum of the markers that were lost and hit the wall, shown in Fig. 6, is dominated by peaks at the three injection energies: 75, 37.5 and 25 keV. As the spectrum suggests, the average CX loss time, which is 2.6 ms, is much shorter than the average slowing-down time, which is 20 ms according to the simulation with CX turned off. This implies that almost all of the beam ions that travel sufficiently close to the separatrix are neutralized by CX. However, due to the randomness of the gyroangle at neutralization, a fraction of the fast atoms travel radially inwards and are reionized deeper inside the plasma. Indeed, of the beam ions born outside $\rho_{\mathrm{pol}} = 0.9$, only an estimated 71% are lost.

The uncertainties from the extrapolation of atomic data proved negligible. The lower limit of the fast-particle energy abscissa in the BMS data is 5 keV/amu, i.e., 10 keV

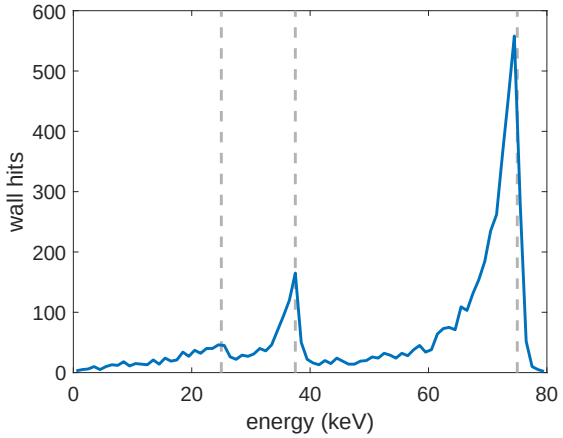

Figure 6: Energy spectrum of ASCOT markers hitting the wall. Injection energies are indicated by the gray dashed lines.

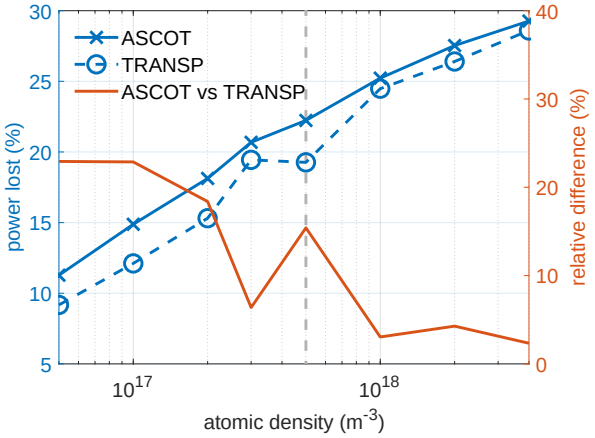

Figure 7: Loss of captured beam power due to CX predicted by ASCOT and TRANSP for various scrape-off-layer atomic densities. The relative difference is shown on a separate scale. Target scenario density is indicated by the gray dashed line.

for deuterium. In the ASCOT simulation, only 1.9% of the markers that hit the wall had energies below 10 keV, based on the data shown in Fig. 6. This further justifies the simplified atomic background, discussed in section 4.1. The plasma density and temperature profiles reach the lower limits of the corresponding abscissae of the BMS data at the separatrix or in the scrape-off layer. Because of the low density and its rapid decrease outwards in the scrape-off layer, ionization is improbable. For the above reasons, the uncertainty from extrapolation of the BMS data is deemed negligible. Since ADAS can generate CX cross-sections for arbitrary collision energies, albeit using extrapolation according to the approach of ADF24, and since the Maxwellian averaging is performed in ASCOT, it was possible to choose the abscissae for the CX rate coefficient such that they cover the relevant domain.

Since the CX process is sensitive to the background atomic density, both the ASCOT and TRANSP simulations were repeated for varied values of the atomic density in the scrape-off layer to assess how uncertainty in the assumed atomic density cascades into uncertainty in the effect of CX on beam ions. Only the input parameter for scrape-off-layer atomic density was changed in TRANSP. Each ASCOT simulation was prepared using the data of the corresponding TRANSP simulation. The dependence of the simulated CX-induced beam power loss on the atomic density, as predicted by ASCOT and TRANSP, is shown in Fig. 7. While the ASCOT prediction is persistently higher, the discrepancy stays within 23% throughout the density range. It is unclear why the TRANSP prediction in the case of the target density deviates from the overall trend.

4.3. Heating and current drive

The loss of beam ions due to CX strongly reduces plasma heating towards the edge. Figure 8 shows the simulated radial profiles of plasma heating, i.e., deposition of power from beam ions to bulk electrons and ions. The heating profiles predicted by ASCOT with and without the inclusion of CX reactions are compared to determine the impact of CX. Inside $\rho_{\mathrm{pol}} = 0.4$, heating is estimated to be reduced by less than 5%. The reduction reaches 20% at $\rho_{\mathrm{pol}} = 0.6$. Outwards, the reduction grows rapidly, reaching a maximum of 80% at the separatrix. The heating profile predicted by ASCOT with CX turned on is also compared to the prediction by TRANSP. Inside $\rho_{\mathrm{pol}} = 0.9$, the codes agree to within 5%. The ASCOT estimate of the total power deposition, including the energy of thermalized beam ions, is 3.9 MW.

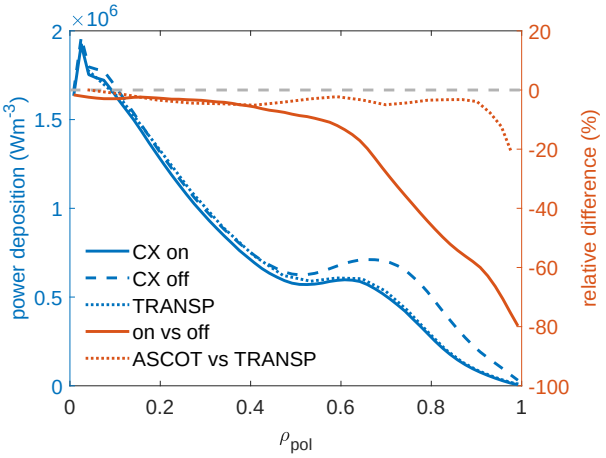

Figure 8: Radial profiles of power deposition from beam ions simulated by ASCOT, with and without the CX model, and by TRANSP. Relative differences are shown on a separate scale.

The beam-ion current drive in the plasma is predicted to decrease towards the edge but increase closer to the core. Figure 9 compares the ASCOT predictions for the electron-shielded current density driven by beam ions with and without the inclusion of CX reactions. Outside $\rho_{\mathrm{pol}} = 0.6$, the current drive is reduced. The reduction increases

towards the edge, reaching a maximum of 80% at the separatrix. Inside $\rho_{\mathrm{pol}} = 0.6$, CX is predicted to increase the current drive, with a maximum increase of 20% observed around $\rho_{\mathrm{pol}} = 0.5$. This increase is explained to result from beam particles that are neutralized by CX closer to the separatrix, or outside it, and are transported inwards and reionized deeper inside the plasma. The inward reach of particles reionized on the low-field side is further extended on the high-field side by the nature of fast-ion orbits in MAST-U, visualized in Fig. 10, thus enabling contribution to current drive deep inside the plasma. The current-drive profile predicted by ASCOT with CX included is also compared to the prediction by TRANSP in Fig. 9. Inside $\rho_{\mathrm{pol}} = 0.8$, the codes agree to within 20%. The ASCOT estimate of the total, area-integrated current drive is 130 kA, which is 12% lower than it would be in the absence of CX reactions.

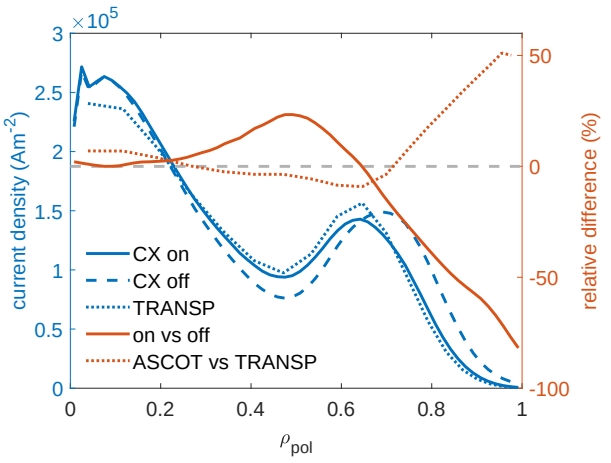

Figure 9: Radial profiles of electron-shielded current drive by beam ions simulated by ASCOT, with and without the CX model, and by TRANSP. Relative differences are shown on a separate scale.

4.4. Wall power loads

In the simulation with 30 times more markers and the 3D wall, to keep the computation time reasonable, the longer time step 10^{-9} s was used. Since the upper limit of the free-path error, 2.7 mm, is still small compared to the mean free paths shown in tables 2 and 3 for relevant plasma densities, and since the purpose of the simulation was a demonstrative estimation of wall power loads, this source of error is deemed acceptable.

Before analyzing the wall deposition of beam particles lost through CX, it is worth pointing out some distinct features of the spherical tokamak geometry of MAST-U, visualized in Fig. 10. The Shafranov shift is pronounced compared to that of a conventional tokamak, leaving flux surfaces considerably closer to the low-field-side separatrix. Furthermore, the strong ∇B and curvature drifts force beam ions towards the plasma core on the high-field side, as illustrated using 2D projections of both the example orbit of a single simulated beam ion and the slowing-down distribution of the ensemble of simulated beam ions. The combined effect of the above features is that beam ions are closest to the edge at the low-field-side midplane while being practically non-existent close to the edge on the high-field side as well as in the top and bottom of the plasma. Moreover, because of the large gyroradii in the weak outboard field, beam ions on confined orbits can travel through the low-field-side scrape-off layer during their gyro-orbits. Given the spatial distribution of the beam ions in the Rz-plane and the strongly peaked radial profile of the thermal atomic density, the birth rate of fast CX atoms is concentrated in the low-field-side scrape-off layer, peaked around the outer midplane, as shown in Fig. 11.

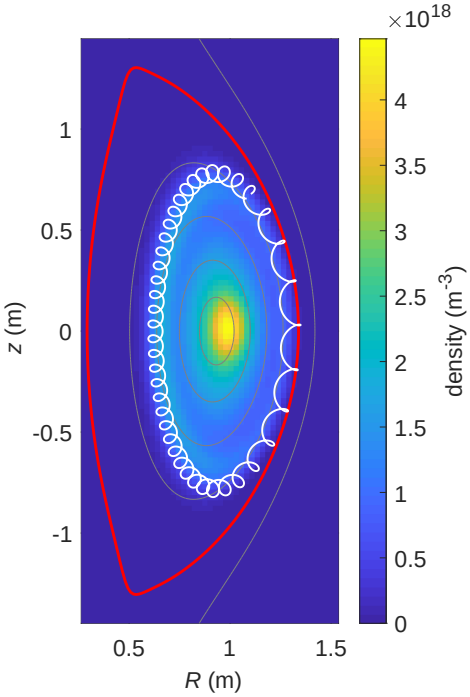

Figure 10: 2D projections of the full gyro-orbit of a passing beam ion (white) and the slowing-down distribution of the ensemble of beam ions simulated by ASCOT. The same flux surfaces are shown as in Fig. 1.

The predicted wall power deposition from beam particles lost through CX is concentrated around the outer midplane. Since a negligible 0.0090% of the power to the wall is in charged particles, scattered randomly around the mouth of the bottom divertor, all of the power to the wall is considered to be in fast CX atoms. While charged particles escaping the plasma are effectively channeled to the divertor, neutral particles penetrate the magnetic field and can reach other regions of the wall. The deposition of fast CX atoms onto the wall depends on their birth distribution. Indeed, the birth distribution shown in Fig. 11 is reflected in Fig. 12, which shows the simulated power loads on a sector of the 3D wall. The wall deposition is concentrated on the central poloidal field coils (P5) and the vacuum vessel wall between them. Quantitatively the

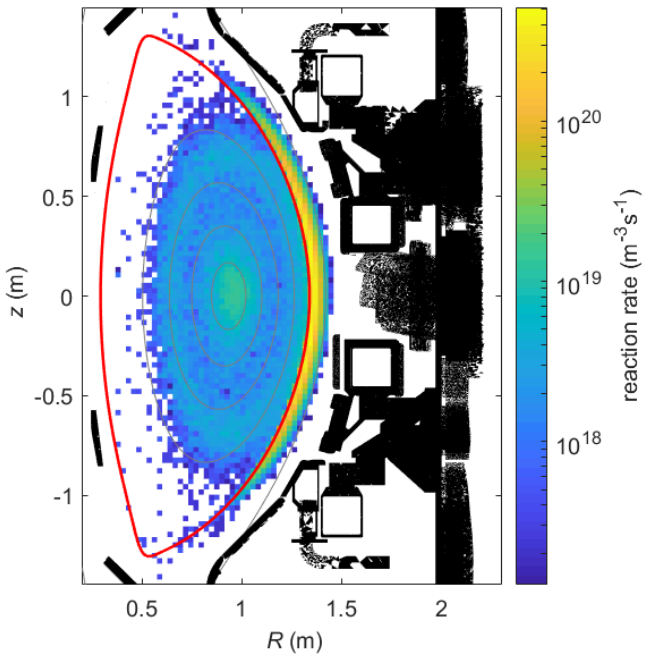

Figure 11: 2D projection of the reaction rate of CX neutralization of beam ions simulated by ASCOT. The same flux surfaces as in Fig. 1 and a 2D projection of the 3D wall (black) are shown.

load differences on these surfaces are small, but qualitatively vertical asymmetry is observed. The highest power loads of 80 $\mathrm{kWm^{-2}}$ are estimated on the lower P5 coil. The upper P5 coil receives peak loads of 70 $\mathrm{kWm^{-2}}$. Between the coils, the vacuum vessel wall, which is closer to the midplane but farther from the plasma, also receives peak loads of 70 $\mathrm{kWm^{-2}}$. Below the lower P5 coil, the power loads on the vacuum vessel are less than 6 $\mathrm{kWm^{-2}}$, and, above the upper P5 coil, less than 3 $\mathrm{kWm^{-2}}$. There is more deposition on the bottom half than on the top half of the tokamak, which is explained by the orientation of the beam-ion orbits in relation to the shape of the plasma. The parallel velocity of a beam ion points upwards and towards the high-field side in the top plasma, and downwards and towards the low-field side in the bottom plasma. Given the shape of the plasma, shown in Fig. 10, fast CX atoms born in the bottom plasma have less plasma to penetrate.

5. Summary and discussion

A new fast-ion CX model has been implemented in the ASCOT fast-ion code. The model was verified by estimating reaction mean free paths. The model was applied to simulate beam ions slowing down in a MAST-U target scenario.

ASCOT simulations with and without the inclusion of CX were compared to gauge its impact on the beam ions. The CX-induced loss of beam power is estimated to be 22%, with 75% of the lost power originating from

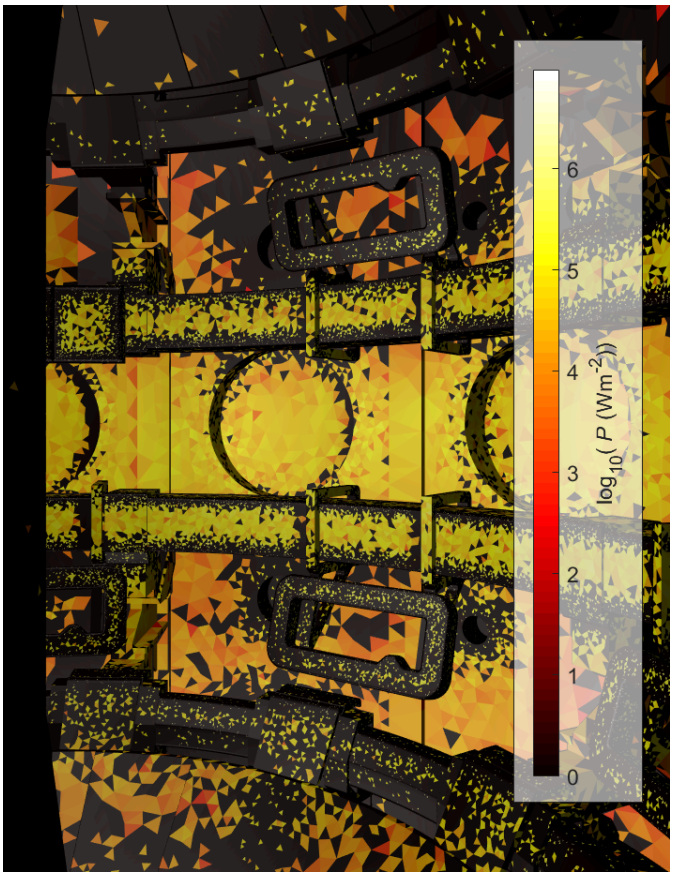

Figure 12: Power loads from fast CX atoms estimated by ASCOT on a sector of the wall.

the off-axis beam. Due to CX, plasma heating and current drive are decreased towards the edge. However, the current drive is increased by up to 20% inside $\rho_{\mathrm{pol}} = 0.6$, resulting in a reduction in the total current drive of 12%. The simulated deposition of fast CX atoms on the wall is concentrated around the outer midplane, with peak power loads of 70–80 $\mathrm{kWm^{-2}}$ on the P5 coils and the vacuum vessel wall between the P5 coils. These results demonstrate the capabilities of ASCOT, with its CX model, to analyze the impact of fast-ion CX on the performance of the plasma and the integrity of plasma-facing components. The background atomic density was assumed poloidally uniform. For future analysis, the transition will be made to 2D atomic background data based on experimental measurements.

As further testing of the ASCOT CX model, the ASCOT predictions were compared to those of TRANSP. The codes agree on the total CX-induced loss of beam power to within 15% in the target scenario, and to within 23% throughout a sensitivity scan spanning a wide range of scrape-off-layer atomic densities. The radial profiles of plasma heating and current drive in the target scenario, when omitting the edge, agree to within 5% and 20%, respectively.

The reason for the modest discrepancies observed be-

tween the predictions of ASCOT and TRANSP is uncertain, but a possible explanation was identified. While TRANSP does use finite-Larmor-radius corrections to account for the gyro-orbit for interactions with the background plasma and atoms, it is fundamentally a guiding-center code and limited to following fast ions inside the confined plasma. As mentioned in section 1, the importance of following the full gyro-orbits of fast ions in MAST has been experimentally demonstrated [3, 11]. Specifically, when compared to TRANSP, full gyro-orbit following by ASCOT yielded predicted neutron emission rates that were quantitatively more consistent with the measurements [11]. The cause of the difference in the predicted neutron rates explains part of the discrepancy observed in the simulated CX losses as well. To validate the ASCOT CX model, it will be compared to experiments in MAST or MAST-U.

Acknowledgements

We thank Ephrem Delabie, Michael Fitzgerald, Marina Gorelenkova, Stuart Henderson, Martin O'Mullane, Juan Rivero-Rodriguez and Samuel Ward for help with codes and data. The ASCOT simulations were carried out on the EUROfusion High Performance Computer, Marconi-Fusion, at CINECA. We acknowledge the computational resources provided by the Aalto Science-IT project. This work has been carried out within the framework of the EUROfusion Consortium and has received funding from the Euratom research and training programme 2014-2018 and 2019-2020 under grant agreement No 633053 and from the RCUK grant No EP/T012250/1. The views and opinions expressed herein do not necessarily reflect those of the European Commission. This work was partially funded by the Academy of Finland project No 328874 and 324759.

References

[1] K. McClements, K. Tani, R. Akers, Y. Liu, K. Shinohara, H. Tsutsui, S. Tsuji-Iio, The effects of resonant magnetic perturbations and charge-exchange reactions on fast ion confinement and neutron emission in the Mega Amp Spherical Tokamak, Plasma Physics and Controlled Fusion 60 (9) (2018) 095005, doi: 10.1088/1361-6587/aad252.

[2] E. Hirvijoki, O. Asunta, T. Koskela, T. Kurki-Suonio, J. Miettunen, S. Sipilä, A. Snicker, S. Äkäslompolo, ASCOT: Solving the kinetic equation of minority particle species in tokamak plasmas, Computer Physics Communications 185 (4) (2014) 1310–1321, doi: 10.1016/j.cpc.2014.01.014.

[3] K. Tani, K. Shinohara, T. Oikawa, H. Tsutsui, K. McClements, R. Akers, Y. Liu, M. Suzuki, S. Ide, Y. Kusama, et al., Application of a non-steady-state orbit-following Monte-Carlo code to neutron modeling in the MAST spherical tokamak, Plasma Physics and Controlled Fusion 58 (10) (2016) 105005.

[4] G. Kramer, R. Budny, A. Bortolon, E. Fredrickson, G. Fu, W. Heidbrink, R. Nazikian, E. Valeo, M. Van Zeeland, A description of the full-particle-orbit-following SPIRAL code for simulating fast-ion experiments in tokamaks, Plasma Physics and Controlled Fusion 55 (2) (2013) 025013.

[5] G. Kramer, M. Van Zeeland, A. Bortolon, Full-orbit simulations of fast-ion charge-exchange losses induced by neutral particles outside the last-closed flux surface, Nuclear Fusion 60 (8) (2020) 086016.

[6] F. Jaulmes, G. Zadvitskiy, K. Bogar, M. Imrisek, J. Hromadka, S. Cats, J. Varju, M. Komm, R. Panek, Modelling of charge-exchange induced NBI losses in the COMPASS upgrade tokamak, Nuclear Fusion 61 (4) (2021) 046012.

[7] R. Goldston, D. McCune, H. Towner, S. Davis, R. Hawryluk, G. Schmidt, New techniques for calculating heat and particle source rates due to neutral beam injection in axisymmetric tokamaks, Journal of Computational Physics 43 (1) (1981) 61–78, doi: 10.1016/0021-9991(81)90111-X.

[8] PPPL TRANSP, `https://transp.pppl.gov/index.html`, accessed: Aug. 10, 2021.

[9] A. Pankin, D. McCune, R. Andre, G. Bateman, A. Kritz, The tokamak Monte Carlo fast ion module NUBEAM in the National Transport Code Collaboration library, Computer Physics Communications 159 (3) (2004) 157–184.

[10] M. Tournianski, R. Akers, P. Carolan, D. Keeling, Anisotropic fast neutral particle spectra in the MAST spherical tokamak, Plasma Physics and Controlled Fusion 47 (5) (2005) 671.

[11] A. Sperduti, M. Cecconello, S. Conroy, A. Snicker, Neutron rate estimates in MAST based on gyro-orbit modelling of fast ions, Nuclear Fusion 61 (1) (2020) 016028.

[12] S. Äkäslompolo, P. Drewelow, Y. Gao, A. Ali, C. Biedermann, S. Bozhenkov, C. Dhard, M. Endler, J. Fellinger, O. Ford, et al., Validating the ASCOT modelling of NBI fast ions in Wendelstein 7-X stellarator, Journal of Instrumentation 14 (10) (2019) C10012.

[13] H. Summers, M. O'Mullane, The Atomic Data and Analysis Structure, in: Nuclear Fusion Research, Springer, 2005, pp. 399–413.

[14] H. Summers, W. Dickson, M. O'Mullane, N. Badnell, A. Whiteford, D. Brooks, J. Lang, S. Loch, D. Griffin, Ionization state, excited populations and emission of impurities in dynamic finite density plasmas: I. The generalized collisional–radiative model for light elements, Plasma Physics and Controlled Fusion 48 (2) (2006) 263–293, doi: 10.1088/0741-3335/48/2/007.

[15] ADAS Atomic Data and Analysis Structure, `http://www.adas.ac.uk`, accessed: July 29, 2021.

[16] P. Sirén, J. Varje, S. Äkäslompolo, O. Asunta, C. Giroud, T. Kurki-Suonio, H. Weisen, et al., Versatile fusion source integrator AFSI for fast ion and neutron studies in fusion devices, Nuclear Fusion 58 (1) (2017) 016023, doi: 10.1088/1741-4326/aa92e9.

[17] S. Smith, S. Pamela, A. Fil, M. Hölzl, G. Huijsmans, A. Kirk, D. Moulton, O. Myatra, A. Thornton, H. Wilson, et al., Simulations of edge localised mode instabilities in MAST-U Super-X tokamak plasmas, Nuclear Fusion 60 (6) (2020) 066021.

[18] R. Goldston, P. Rutherford, Introduction to Plasma Physics, Inst. of Phys Publ. (1995).

[19] J. Varje, K. Särkimäki, J. Kontula, P. Ollus, T. Kurki-Suonio, A. Snicker, E. Hirvijoki, S. Äkäslompolo, High-performance orbit-following code ASCOT5 for Monte Carlo simulations in fusion plasmas, arXiv preprint arXiv:1908.02482 (2019).

[20] S. Suzuki, T. Shirai, M. Nemoto, K. Tobita, H. Kubo, T. Sugie, A. Sakasai, Y. Kusama, Attenuation of high-energy neutral hydrogen beams in high-density plasmas, Plasma Physics and Controlled Fusion 40 (12) (1998) 2097–2111, doi: 10.1088/0741-3335/40/12/009.

[21] H. Anderson, M. von Hellermann, R. Hoekstra, L. Horton, A. Howman, R. Konig, R. Martin, R. Olson, H. Summers, Neutral beam stopping and emission in fusion plasmas I: deuterium beams, Plasma Physics and Controlled Fusion 42 (7) (2000) 781–806, doi: 10.1088/0741-3335/42/7/304.

[22] E. Delabie, M. Brix, C. Giroud, R. Jaspers, O. Marchuk, M. O'Mullane, Y. Ralchenko, E. Surrey, M. Von Hellermann, K. Zastrow, et al., Consistency of atomic data for the interpretation of beam emission spectra, Plasma Physics and Controlled Fusion 52 (12) (2010) 125008.

[23] NTCC PSPLINE Module, `https://w3.pppl.gov/ntcc/PSPLINE/`, accessed: Aug. 10, 2021.

[24] M. Matsumoto, T. Nishimura, Mersenne twister: a 623-dimensionally equidistributed uniform pseudo-random number generator, ACM Transactions on Modeling and Computer Simulation (TOMACS) 8 (1) (1998) 3–30, doi: 10.1145/272991.272995.

[25] P. Ollus, Modelling charge exchange losses of beam ions in the MAST-U spherical tokamak, Master's thesis (Nov. 2019).

[26] A. Morris, MAST: Results and Upgrade Activities, IEEE Transactions on Plasma Science 40 (3) (2012) 682–691, doi: 10.1109/tps.2011.2181540.

[27] D. Keeling, T. Barrett, M. Cecconello, C. Challis, N. Hawkes, O. Jones, I. Klimek, K. McClements, A. Meakins, J. Milnes, et al., Mitigation of MHD induced fast-ion redistribution in MAST and implications for MAST-Upgrade design, Nuclear Fusion 55 (1) (2014) 013021.

[28] MAST-U Machine Description, `https://users.mastu.ukaea.uk/machine-description`, accessed: Sept. 30, 2021.

[29] TRANSP Help, `https://w3.pppl.gov/~pshare/help/transp.htm`, accessed: July 23, 2021.